20th Australasian Fluid Mechanics Conference
Perth, Australia
5-8 December 2016

Effect of Air Ingestion at the Start of Injection Process in a Diesel Injector

M. Ghiji[1], L. Goldsworthy[1], P.A. Brandner[1], V. Garaniya[1], and P. Hield[2]

[1]Australian Maritime College
University of Tasmania, Launceston, Tasmania, 7250, Australia

[2]Defence Science and Technology Group
Melbourne, Victoria, 7307, Australia

Abstract

The effect of the presence of air in the injector nozzle at the Start of Injection (SOI) in a single-hole high-pressure diesel injector is investigated experimentally and numerically. Experimental measurements are performed using a laser-based backlit imaging technique through a long distance microscope. Numerical investigation of, in- and, near-nozzle fluid dynamics is conducted in an Eulerian framework using a Volume of Fluid interface capturing technique integrated with Large Eddy Simulation (LES) turbulence modelling. Experimental images show transparency in the emerging jet suggesting the presence of air trapped inside the nozzle liquid from the previous injection event. The numerical model provided a clearer insight into the influence of air on the structure and dynamics of an emerging jet at the SOI. A mathematical code is developed to replicate the backlit imaging approach with the numerical results. The virtual images demonstrate a transparent liquid jet emerging into the pressurised spray chamber gas, in improved agreement with the experimental images. The inclusion of air in the nozzle prior to injection in the numerical model also yields improved agreement in the penetration velocity profile of the jet. These results explain how air inclusion inside the nozzle liquid affects the physics of the penetrating jet at the SOI. The air inclusion also provides an explanation for not only the transparency of the emerging jet but also rough interfacial surfaces captured at the very early stages of injection.

Introduction

Diesel engines are fed by injectors which supply fuel to chambers where its internal energy is converted to heat through a combustion process driving the pistons and finally delivering the torque to the propulsion system. The quality of air-fuel mixture is mainly controlled by the injector performance, governing the combustion process, engine power and ultimately emissions formation [7]. The atomisation of liquid jet can be improved by increasing the injection pressure, currently up to 3000 bar in compression ignition (diesel) engines. At such a high injection pressures fuels experience temporal, spatial, and physical transient behaviours such as cavitation; evaporation, turbulence, and surface energy effects due to intricate physics involved in and outside of the injector [7]. Based on the Reynolds and Weber/Ohnesorge numbers of the injected fuel in diesel engines the breakup of liquid jets falls well within the atomisation regime. In such a regime, average droplet diameters and scale of flow instabilities are much smaller than the jet diameter. With the aid of recent developments in experimental measurements such as X-ray technologies and high-speed cameras, researchers can conduct detailed analyses to gain clearer insights into the simultaneous and interactive complex physics associated with liquid fuel atomisation.

Application of the Large Eddy Simulation (LES) allows large-scale eddies which contain a more universal energy, to be resolved while small scale eddies are filtered and then modelled by a turbulence model. For Reynolds Averaged Navier-Stokes (RANS) models, less computation time is required because of their averaging approach, diminishing some features of the transient spray structure and the sharp interfaces [3, 7]. Moreover, it is vital to accurately capture the transient behaviour of interfaces as it plays a determining role in the separation and breakup process of a liquid jet. Some numerical techniques reconstruct the liquid-gas interfaces by tracking them explicitly such as the Volume of Fluid (VOF) or Level-Set approach while other techniques utilize a diffuse-interface modelling approach where the interfaces are not explicitly trackable and only partially resolved by a high-resolution grid [7]. Conventional atomisation models predict the breakup process through a Lagrangian framework neglecting background fluid flow effects on droplets and the limitation of grid refinement [3]. An overview of numerical methods suggests the use of the Eulerian/LES/VOF approach in the characterization of, in- and, near-nozzle flow structures.

X-ray imaging of the closing transient in a diesel injector by Swantek *et al.* [9] depicts some gas bubbles ingested in the nozzle and sac. They proposed that the bubbles are due to air ingestion rather than cavitation in the bulk fluid. Further studies [1, 2, 9] provide a better understanding of the influence of factors such as nozzle hole size, rail injection and spray chamber pressure on the air ingestion mechanism during the End of Injection (EOI) process. They found that the air trapped inside the nozzle is due to the high inertia of the internal flow exiting the nozzle at EOI. Moreover, recent measurements of the early stages of injection in a high-pressure spray chamber by the authors [5, 6] suggest that the transparency of the emerging jet at the SOI is due the presence of air in the first injected fuel, which is likely to be due to air ingestion at the EOI of the previous shot. The ingested air at the EOI affects the fuel penetration and evaporation rate of the next injection event specifically during the first 100 μs after the SOI which subsequently leads to partial combustion and ultimately increase in the production of pollutants [8, 9]. These drawbacks have motivated many researchers to investigate, comprehend and finally optimize the parameters and physics associated with EOI process. Details of these extremely transient phenomena and their corresponding effects are a challenging subject and yet to be fully understood.

The present study focuses on experimental and numerical investigations of the effect of air ingestion processes occurring at the EOI on the general structure of an emerging jet in a single-hole sharp edged nozzle at the SOI. A key aim of the present work is to investigate the source of qualitative deviation between previous experimental and numerical images by including more realistic initial conditions in numerical models. A further aim is to enhance understanding of, in- and, near-nozzle processes.

Methodology

Experimental apparatus

Experimental tests are conducted by spraying a high-pressure diesel fuel axially through a single solid cone injector from the top of a constant volume High-Pressure Spray Chamber (HPSC). The structure of emerging jet at the early stage of injection has been capturing using a microscopic laser-based backlight imaging (shadowgraphy) technique. The injection pressure profile is highly repeatable from shot to shot, and is increased to 1200 bar at the quasi-steady stage of injection. Detailed specifications and settings of utilized instruments are provided in Ghiji *et al.* [5, 6]. Captured experimental images are used to evaluate and then validate the numerical results.

Mathematical Method

In this study, the VOF phase-fraction based interface capturing technique is employed in the open source numerical code OpenFOAM v2.3. The governing equations of the solver (compressibleInterFoam) consist of the balances of mass (1), momentum (2), total energy (3), and the equation of state (10) for two immiscible, compressible fluids with the inclusion of the surface tension between the two phases. The basic form of the governing mass, momentum, and energy conservations are:

$$\frac{\partial \rho}{\partial t} + \nabla.(\rho \boldsymbol{V}) = 0 \tag{1}$$

$$\frac{\partial \rho \boldsymbol{V}}{\partial t} + \nabla.(\rho \boldsymbol{V}\boldsymbol{V}) = -\nabla p + \nabla.\tau + \rho \boldsymbol{g} + \int_{S(t)} \sigma \boldsymbol{\kappa} \boldsymbol{n} \delta(x - x')dS \tag{2}$$

$$\frac{\partial \rho \widehat{U}}{\partial t} + \nabla.\left(\rho \widehat{\boldsymbol{U}} \boldsymbol{V}\right) + \frac{\partial \rho \boldsymbol{K}}{\partial t} + \nabla.(pK\boldsymbol{V}) + \nabla.(p\boldsymbol{V}) = -\nabla.\mathrm{q} - \nabla.(\tau.\boldsymbol{V}) + \rho \boldsymbol{g}.\boldsymbol{V} \tag{3}$$

Where ρ is the density, V is the velocity, p is the pressure, t is the time, τ is the stress tensor, κ is the local curvature of the liquid surface, internal energy $\widehat{U}$, and and, n denotes a unit vector normal to the liquid surface S. The operators $\nabla(\,)$ and $\nabla.(\,)$ represent the gradient and the divergence operations, respectively. The integral term in equation (2) represents the momentum source due to surface tension force on the interface $S(t)$. This force only acts on S, as ensured by the indicator function $\delta(...)$. The momentum source due to surface tension force on the interface $S(t)$, the integral term in equation (2), only acts on S and produces a non-zero value when $x = x'$ which is an indication of the existence of an interface. The estimation of this integral term is obtained through the continuum surface force model as:

$$\int_{S(t)} \sigma \boldsymbol{\kappa} \boldsymbol{n} \delta(x - x')dS \approx \sigma \boldsymbol{\kappa} \nabla.\gamma \tag{4}$$

where γ is the volume fraction of the liquid phase defined as

$$\gamma = \begin{cases} 1 & \text{for a point inside the liquid} \\ 0 < \gamma < 1 & \text{for a point inside the transitional region} \\ 0 & \text{for a point inside the gas} \end{cases} \tag{5}$$

The 'transitional region' is where the interface is located, realized as an artefact of the numerical solution process. Fluid in the transition region is considered as a mixture of the two fluids on each side of the interface, which cannot completely resolve a discontinuous step. The two-phase flow field is treated as a single incompressible continuum with an effective local density ρ, and viscosity μ estimated based on volume fraction of a computational cell as:

$$\rho = \gamma \rho_l + (1 - \gamma)\rho_g \tag{6}$$

$$\mu = \gamma \mu_l + (1 - \gamma)\mu_g \tag{7}$$

The subscripts l and g represent the liquid and gas phases respectively. The volume fraction is obtained from the solution of a transport equation:

$$\frac{\partial \rho \gamma}{\partial t} + \nabla.(\rho V \gamma) = 0 \tag{8}$$

The interface curvature, κ, is calculated by

$$\boldsymbol{\kappa} = \nabla.\left(\frac{\nabla \gamma}{|\nabla \gamma|}\right) \tag{9}$$

The system of equations are closed by an equation of state

$$\begin{cases} \rho_l = p\,\psi_l \\ \rho_g = p\,\psi_g \end{cases} \tag{10}$$

where ψ is the compressibility. The interfacial surface $S(t)$ is captured and tracked using a VOF technique which utilizes a "compression velocity" term in equation (8) to preserve sharp interfaces. The LES/VOF equations are derived from equations (1), (2), and (8) using localized volume averaging of the phase-weighted hydrodynamic variables. This process, known as filtering, includes decomposition of the relevant variables into resolvable and sub-grid scales of turbulent fluctuations. This filtering together with the non-linear convection terms in equation (2) introduce an additional quantity, known as the sub-grid scale (SGS) stresses τ^{sgs}. The SGS stresses comprise correlation of the variable fluctuations at sub-grid scales that entail closure through mathematical models as:

$$\tau^{sgs} = \overline{\boldsymbol{V}\boldsymbol{V}} - \overline{\boldsymbol{V}}\,\overline{\boldsymbol{V}} \tag{11}$$

and estimated by a sub-grid scale model of the eddy-viscosity type as:

$$\tau^{sgs} - \frac{2}{3}\,k\,\boldsymbol{I} = -\frac{\mu^{sgs}}{\rho}\,(\nabla \overline{\boldsymbol{V}} + \nabla \overline{\boldsymbol{V}}^T) \tag{12}$$

where I is the identity tensor, k is the sub-grid scale turbulent energy and μ^{sgs} is the sub-grid scale viscosity. Both are determined from the one-equation SGS turbulent energy transport model:

$$\frac{\partial k}{\partial t} + \nabla.(k\bar{V}) = \nabla.[(\vartheta + \vartheta^{sgs})\nabla k + \tau^{sgs} \cdot \bar{V}] - \varepsilon - \frac{1}{2}\tau^{sgs} : (\nabla \bar{V} + \nabla \bar{V}^T) \tag{13}$$

where $\varepsilon = C_\varepsilon \rho\, k^{(3/2)}/\Delta$ is the SGS turbulent dissipation $\vartheta^{sgs} = C_k \rho\, k^{(1/2)}/\Delta$ is the SGS kinematic viscosity and $\Delta = V^{(1/3)}$ is the filter width where V is the cell volume. The coefficients are $C_\varepsilon = 1$ and $C_k = 0.05$.

Second-order spatial and temporal discretization schemes are employed by an implicit finite-volume method to solve mathematical models. Pressure Implicit with Split Operator (PISO) algorithm, together with conjugate gradient methods for coupled solution of mass and momentum conservation equations are used. The advection terms are solved by a bounded Normalized Variable (NV) Gamma differencing scheme with a blending factor of 0.2 and the interface compression scheme (CICSAM) for capturing sharp immiscible interfaces. A conservative, bounded, Gauss linear second order scheme is used for Laplacian derivative terms with an additional explicit corrector for mesh non-orthogonality. A second order, implicit discretization scheme, *backward*, is used for the time derivative terms.

Boundary Conditions and Initial Setup

The 3D computational domain has been generated based on the geometry of the experimental nozzle, as shown in Figure 1, revealed by X-ray Computer-Aided Tomography analysis by the

Centre for Materials and Surface Science and the Centre of Excellence for Coherent X-ray Science at La Trobe University. Special considerations take into account in the generation of structured hexahedral mesh at atomisation region and no-slip walls. With the aim of previous mesh sensitivity studies [4-6], results of only a fine mesh with 20 million cells are presented. The cell size is down to 0.1 µm in the nozzle (in the order of the Kolmogorov length scale for the liquid phase) and 1.7 µm in the primary atomisation zone, enables capturing droplets as small as 3 µm diameter.

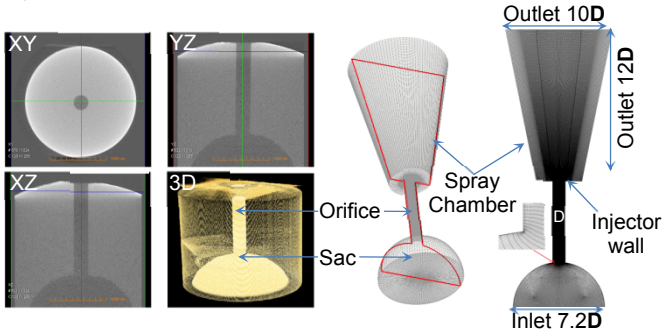

Figure 1. Left: X-Ray tomography measurements of sac and nozzle (orifice) geometry. Middle: the structured hexahedral mesh based on X-ray measurements. Right: a cross-section of the computational domain presents the mesh refinements, dimensions, and condition of the boundaries. The nozzle inlet is sharp edged.

Fuel properties and test setup conditions are listed in Table 1. All experimental and numerical settings, operating and boundary conditions, and injection pressure profiles are replicated based on M.Ghiji *et al.* [6]. The position of the liquid-gas interface and ingested air trapped inside the nozzle liquid from previous injection events determined by the EOI simulation. Final results of the EOI model are used to initialize the present simulation in order to provide clearer insights into the influence of air ingestion mechanisms on the spray structure at the early stage of injection.

Parameter	Value
Injection pressure	120 MPa average (quasi-steady)
Nozzle diameter	0.25 mm
Nozzle length	1.6 mm
Nozzle nominal geometry	$K_S = 0$ (cylindrical)
Fuel	Diesel
Diesel fuel density	832 kg/m^3
Gas Chamber pressure	Air, 30 bar
Density ratio	42
Fuel Kinematic viscosity	2.52×10^{-6} m^2/s
Surface tension	0.03 N/m
Temperature	25°C
Fuel Re_l at the SOI	$5600 \leq Re \leq 13400$

Table 1. Fuel properties and experimental operating conditions. The nozzle diameter is used as the length scale.

Results and Discussions

The experimental images, Figure 2-a and b, illustrate a starting vortex in the chamber near the nozzle exit before the emergence of the fuel [5], suggesting a partially filled nozzle. Moreover, transparency in the emerging jet can be seen in Figure 2-c and d due to the emergence of trapped air inside the nozzle liquid from the previous injection event [6]. Numerical results without the air inclusion, Figure 2-e and f, show no sign of the transparency while Figure 2-g and h show the transparency inside the emerging jet where trapped air is pushing away and expanding the leading edge of the jet. Numerical images with the air inclusion, Figure 2-g and h are montaged based on a developed mathematical code which replicates the shadowgraphy approach. This code first evaluates the value of each pixel of a virtual backlit greyscale image over 20 stream-wise cut-planes of the jet and then averages these pixel intensities in a single image.

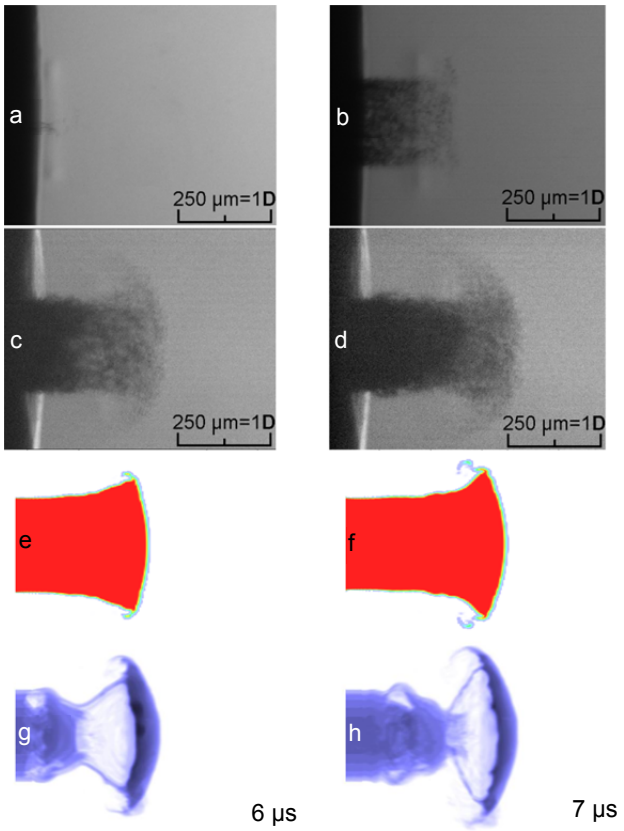

Figure 2. Experimental results of the starting vortex just before (image a) and just After the Start of Penetration (image b); image c and d are from a single shot with 1 µs inter-frame time show some transparency at the leading edge; image e, f and g, h depict the CFD results without and with air inclusion respectively at 6 and 7 µs ASOP. CFD results in image g and h are averaged over 20 centred cross-sectional planes.

The numerical and experimental results show the early development of the umbrella-shaped leading edge structure and the early stages of shedding of droplets from the rim of the leading edge. Shadowgraphy images are compared with numerical results in Figure 3, presenting the general structure of the diesel spray. In this Figure, images (a) and (b), (d) and (e), (g) and (h), (i) and (j) are paired, each pair captured from a single injection event with 1 µs delay between two consecutive frames.

The emergence of trapped air from previous injection events significantly alters the morphology of the spray. A ragged interfacial surface can be seen even at the very early stage of jet appearance. The tip of the jet leading edge is more oblique and the necking of the jet behind the umbrella in Figure 3 is, in better agreement with experimental results in comparison with earlier numerical images [5]. The partial transparency of the experimental and numerical images can be seen leading to a more rapid disintegration. Despite the previous studies by the authors [4-6] where the influence of trapped air had been neglected, the production of small droplets commence at very early stages of the jet penetration.

Experimental and numerical penetration velocity of the jet at different axial distances from the nozzle exit and the corresponding Reynolds numbers are shown in Figure 4. Experimental values are calculated by considering the displacement of the leading edge and the time-interval between two successive shots. The increase in the injection pressure in the sac, determined by the injection pressure ramp at the sac inlet, results in an overall rise in the penetration velocity and Reynolds number. The more realistic initial conditions at the start of simulation (inclusion of ingested air inside the nozzle liquid) lead to better agreement with the experimental data.

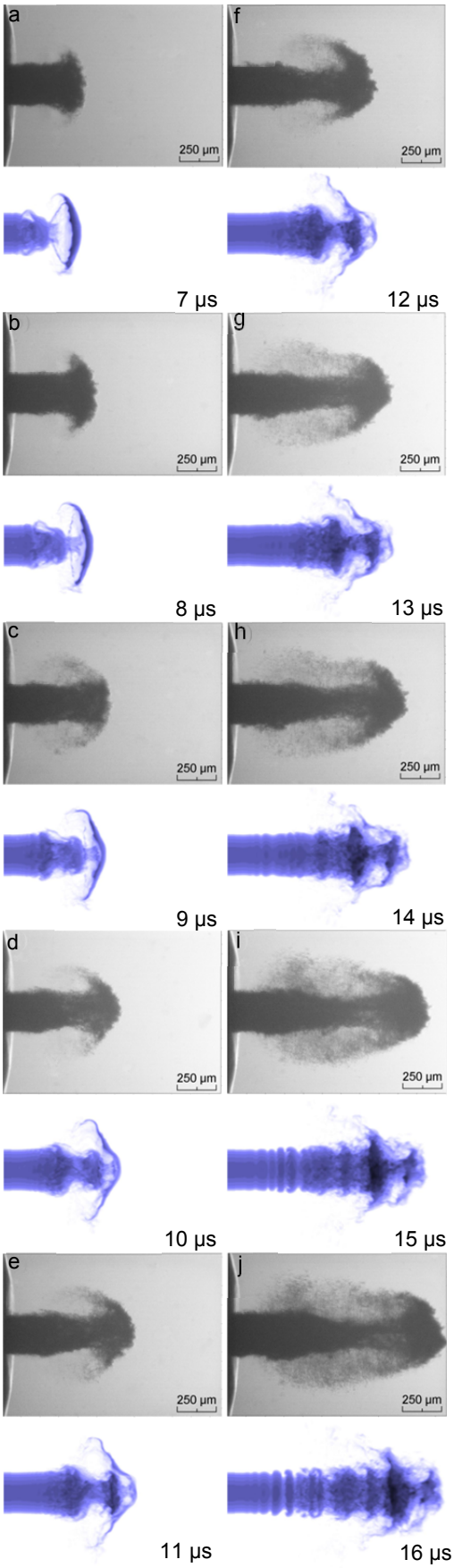

Figure 3. Comparison of experimental images with CFD results. Images a and b, d and e, g and h, i and j are paired, each pair captured from the same injection event with 1 µs inter-frame time. Numerical results show the structure of the liquid at corresponding times ASOP.

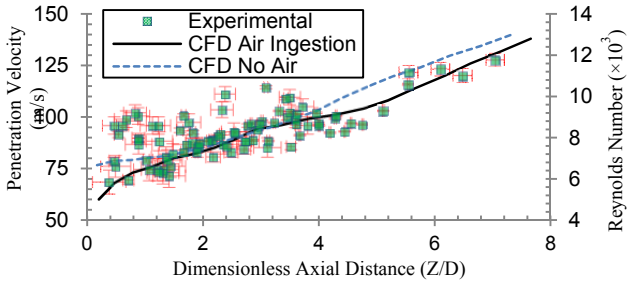

Figure 4. Experimental and numerical values of penetration velocity of the leading edge at various axial distances from the nozzle exit. Inclusion of air in the initial conditions of simulation shows a better agreement compared with the just partially filled nozzle [5]. Reynolds number values are correlated using the computed penetration velocity of the leading edge.

Conclusions

The effect of ingested air, trapped from previous injection shots, on early stage of diesel spray dynamics is investigated experimentally and numerically employing microscopic backlit imaging and Eulerian/LES/VOF modelling respectively. The effects of trapped air on the growth and disintegration of surface structures on the emerging jet are characterized providing insight into the physics of primary atomisation. At the start of penetration, an umbrella-like leading edge and a semi-transparent cloud of air-fuel mixture at the leading edge are captured in both the numerical and experimental data. Comparison of measured penetration velocity of the jet between more than 100 consecutive shots and numerical results shows better correlation between experimental results and previous numerical results. The numerical results support the conclusion that air ingestion phenomena at the EOI significantly affect the spray structures and dynamics.

Acknowledgments

The authors acknowledge the support of the Australian Maritime College and the Defence Science and Technology Group.

References

[1] Battistoni, M., C. Poggiani, and S. Som, Prediction of the Nozzle Flow and Jet Characteristics at Start and End of Injection: Transient Behaviors. *SAE International Journal of Engines*, 2015. 9(2015-01-1850).

[2] Battistoni, M., Q. Xue, and S. Som, Large-Eddy Simulation (LES) of Spray Transients: Start and End of Injection Phenomena. *Oil & Gas Science and Technology*, 2016. 71(1): p. 4.

[3] Bong, C.H., Numerical and experimental analysis of diesel spray dynamics including the effects of fuel viscosity, in *Australian Maritime College,* 2010, University of Tasmania.

[4] Ghiji, M., et al. CFD Modelling of Primary Atomisation of Diesel Spray. in *19th Australasian Fluid Mechanics Conference*. 2014.

[5] Ghiji, M., et al., Analysis of Diesel Spray Dynamics using a Compressible Eulerian/VOF/LES Model and Microscopic Shadowgraphy. *Fuel*, 2016. 188: p. 352-366.

[6] Ghiji, M., et al., Numerical and experimental investigation of early stage diesel sprays. *Fuel*, 2016. 175: p. 274–286.

[7] Jiang, X., et al., Physical modelling and advanced simulations of gas–liquid two-phase jet flows in atomization and sprays. *Progress in Energy and Combustion Science*, 2010. 36(2): p. 131-167.

[8] Pickett, L.M., et al., Transient rate of injection effects on spray development, 2013, *SAE Technical Paper*.

[9] Swantek, A.B., et al., End of Injection, Mass Expulsion Behaviors in Single Hole Diesel Fuel Injectors, in *ILASS Americas 26th,* 2014: Portland, OR, USA.